Vorontsov, V. A., Shen, C., Wang, Y., Dye, D., & Rae, C. M. F. (2010).
Shearing of γ́ precipitates by a (112) dislocation ribbons in Ni-base superalloys: a phase field approach.
Acta Materialia, 58(12), 4110-4119.
https://doi.org/10.1016/j.actamat.2010.03.041

Shearing of γ' Precipitates by $a\langle 112\rangle$ Dislocation Ribbons in Ni-Base Superalloys: A Phase Field Approach

V.A. Vorontsov [a], C. Shen [b], Y. Wang [c], D. Dye [d] and C.M.F. Rae [a]

[a] *Department of Materials Science and Metallurgy, University of Cambridge, Pembroke Street, Cambridge, CB2 3QZ, UK*

[b] *GE Global Research, Niskayuna, NY, 12309, USA*

[c] *Department of Materials Science and Engineering, The Ohio State University, 2041 College Road, Columbus, OH 43210, USA*

[d] *Department of Materials, Royal School of Mines, Imperial College, Prince Consort Road, South Kensington, London SW7 2BP, UK*

Abstract

The "phase field microelasticity theory of dislocations" has been used to study the propagation of dislocation ribbons with an overall Burgers vector of $a\langle 112\rangle$ through a simulated Ni-base superalloy. The driving force for dislocation dissociation reactions and formation of planar faults is incorporated into the free energy using γ-surface functions specially fitted to *ab initio* data. The model shows that the mechanism of cutting of the γ' precipitates by these ribbons exhibits significant dependence on stress magnitude, orientation and precipitate shape. In the case of mixed screw-edge ribbons a change of shearing mode is observed, from stacking fault shear to APB shear, when the applied stress approaches the yield of the material. This transition is absent in pure edge ribbons.

Key words: Primary creep; Dislocation dissociation; Phase field; Shockley partials; Stacking faults

1 Introduction

The superb creep resistance of nickel-base superalloys makes them the materials of choice for manufacturing gas turbine blades. During operation, these components experience a wide range of stresses and temperatures throughout, which limit their service life.

Superalloys exhibit three distinct creep regimes [1]; rafting at high temperatures and low stresses where the microstructure evolves in response to the applied stress; tertiary creep at intermediate temperatures and stresses where dislocation activity is confined solely to the γ matrix; and primary creep at low temperatures and high stresses where dislocations propagate through both phases. Primary creep has been the chief focus of this work. It occurs to a significant extent in the 'cold' webs of cooled HP blades of aero-engines during take-off, climb and thrust reversal routines.

Primary creep occurs in 2^{nd} generation superalloys at 750-850°C when a threshold stress of $\approx$ 500MPa is exceeded [2]. This temperature-dependent threshold stress correlates directly to the ability of $a\langle 112\rangle$ dislocation ribbons to nucleate in the γ matrix, then enter and shear γ' precipitates. A minimum amount of prior plastic deformation of the matrix is required to populate it with a sufficient density of $\frac{a}{2}\langle 110\rangle$ dislocations, which are necessary to form the ribbon. Due to the relatively large length of the $a\langle 112\rangle$ Burgers vector, the propagation of $a\langle 112\rangle$ ribbons introduces a large amount of primary creep strain.

The phase field microelasticity (PFM) theory of dislocations [3] is an attractive approach to treating dislocation problems. A dislocation loop with Burgers vector b_i and slip plane normal n_j can be treated as a coherent misfitting platelet inclusion of thickness d equal to the slip-plane spacing. Its invariant plane strain is equal to the misfit strain ε^0_{ij}. Incorporating this transformation strain tensor into the elastic free energy term allows the dislocation propagation/interaction problem to be treated as growth/interaction of martensitic platelets in an anisotropic medium (with additional physical conditions applied).

$$\varepsilon^0_{ij} = \frac{b_i n_j}{d} \tag{1}$$

In PFM, dislocations are represented by boundaries between slipped and non-slipped regions. The overall state of the system is described by a set of density functions (field variables). Non-zero values of the variables imply slip.

PFM allows incorporation of fault energy data in the form of a periodic γ-surface into the free energy functional [4]. This permits treatment of arbitrary configurations of perfect/partial dislocations and faults within the same framework.

This work presents an investigation into dislocation reactions produced by PFM and their dependence on the applied stress during shearing of γ'. It also compares the results with existing hypotheses based on experimental observations.

2 Model Formulation and Procedure

Let us consider an anisotropic elastic crystal containing a population of dislocations. In PFM, the total free energy F_{total} of such a system is defined by four contributing terms, where W is mechanical work done by the applied stress :

$$F_{total} = F_{elastic} + F_{gradient} + F_{crystal} - W \tag{2}$$

The elastic free energy contribution $F_{elastic}$, describes the long range interactions between the elastic strain fields (lattice distortions) associated with the dislocation loops. Such interactions include mutual attraction or repulsion between individual dislocation loops or segments of the same loop. The model uses principles of the Khachaturyan-Shatalov (KS) [5] theory to resolve the strain energy of the system. Building on the classic work of Eshelby [6], which gives solutions for coherent ellipsoidal inclusions using Green's functions, KS theory is able to solve arbitrary systems of inclusions through Fourier transforms. The elastic free energy functional implemented in the model is the same as that formulated in [3].

The gradient free energy term $F_{gradient}$, gives the excess energy associated with the spatial non-uniformity of the simulated system. It describes the local elastic energy associated with the core of the dislocations. In the model, the state of the system is evaluated at discrete points in 3D space. Hence, minimisation of the gradient energy carries out the finite difference part of simulation. The formulation of the $F_{gradient}$ term used in this study is described in [4]. The particular form, also pays a contribution to the diffuseness of the dislocation core, in compliance with the diffuse interface requirement of PFM.

The role of the crystal free energy $F_{crystal}$ is to provide a periodic potential that arises in the crystal in response to localised plastic shear strain in a slipped region. It serves the same purpose as misfit energy used in the Peierls model. The work of Shen and Wang [4] allowed for the incorporation of γ-surface functions $\gamma(\eta)$ into $F_{crystal}$. This energy term, depending on its definition, determines the core structure of the dislocations in the simulated crystal. The density functions η describe the displacement components along the principal Burgers vectors of the slip system. In FCC crystals there are four primary slip systems. Each has three principal burgers vectors. In this study, dislocation activity on only the (111) slip plane was considered. Hence, the state of the system at any position in space $\mathbf{r}$ is described by just three field variables η_1, η_2 and η_3.

$$F_{crystal} = \int \frac{\gamma(\eta_1, \eta_3, \eta_3)}{d} d\mathbf{r} \tag{3}$$

Two γ-surface functions $\gamma(y, z)$ were used to determine the dislocation-fault

Table 1
Coefficients used to match each the crystalline energy term to the relevant γ-surface in phase field.

Phase	c_0	c_1	c_2	c_3	c_4	c_5	c_6	c_7	c_8	c_9	c_{10}	c_{11}
Ni_3Al	728.7	-127.9	60.5	-164.7	7.2	-3.2	-22.1	207.2	-285.0	2.2	6.6	18.8
Ni	376.2	-107.8	-15.3	-4.4	1.1	0	0	-102.2	35.9	8.8	0	0

configuration that formed in each of the alloy phases. The coordinates y and z give the displacement components along $[\bar{1}2\bar{1}]$ and $[10\bar{1}]$ directions respectively. The functions were fitted to data for pure Ni and Ni_3Al to define the dislocation dissociation in γ and γ' respectively. Each function is a specially constructed Fourier series, matched to twelve key symmetry points on the γ-surface by fitting the twelve coefficients $c_0 - c_{11}$ shown in Table 1. The periodicity constants are $p = 2\pi/(\sqrt{3}b)$ and $q = 2\pi/b$, where $b = a/\sqrt{2}$ and a is the lattice parameter. The data for Ni_3Al as well as the fitting approach were taken from Schoeck *et al.* [7,8]. An alteration was made to the SISF energy, which was lowered to $10\,\mathrm{mJ\,m^{-2}}$, based on TEM observations of Veyssiére *et al.* [9] recommended by Mills [10]. The data for pure Ni was provided by Li [11].

$$
\begin{aligned}
\gamma(y,z) = c_0 &+ c_1[\cos(py)+\cos(0.5py+0.5qz)+\cos(0.5py-0.5qz)] \\
&+ c_2[\cos(qz)+\cos(1.5py+0.5qz)+\cos(1.5py-0.5qz)] \\
&+ c_3[\cos(2py)+\cos(py+qz)+\cos(py-qz)] \\
&+ c_4[\cos(2.5py+0.5qz)+\cos(2py+qz) \\
&+ \cos(0.5py+1.5qz)+\cos(0.5py-1.5qz) \\
&+ \cos(2py-qz)+\cos(2.5py-0.5qz)] \\
&+ c_5[\cos(3py)+\cos(1.5py+1.5qz)+\cos(1.5py-1.5qz)] \\
&+ c_6[\cos(4py)+\cos(2py+2qz)+\cos(2py-2qz)] \\
&+ c_7[\sin(py)-\sin(0.5py+0.5qz)-\sin(0.5py-0.5qz)] \\
&+ c_8[\sin(2py)-\sin(py+qz)-\sin(py-qz)] \\
&+ c_9[\sin(2.5py+0.5qz)-\sin(2py+qz) \\
&- \sin(0.5py+1.5qz)-\sin(0.5py-1.5qz) \\
&+ \sin(2py-qz)+\sin(2.5py-0.5qz)] \\
&+ c_{10}[\sin(3py)-\sin(1.5py+1.5qz)-\sin(1.5py-1.5qz)] \\
&+ c_{11}[\sin(4py)-\sin(2py+2qz)-\sin(2py-2qz)]
\end{aligned}
\tag{4}
$$

Figure 2 shows the contour plot of each function. The incorporated γ-surfaces dictate the local energy minimisation that occurs in the system. To obtain the lowest energy configuration the dislocations would attempt to preferentially dissociate in such a way, that their constituent Burgers vectors pass through the local minima of the γ-surface and the saddle points between them.

The minimisation of fault energy is in competition with minimisation of overall dislocation line length. Consequently, shearing of γ' by extended dislocations will prevail at lower values of stress, because anti-phase boundary (APB) energy presents a greater obstacle.

The pure nickel γ-surface predicts dissociation of perfect $\frac{a}{2}\langle 110\rangle$ dislocations into Shockley partial pairs binding an intrinsic stacking fault (ISF). In Ni_3Al, which has $L1_2$ structure, the perfect $\frac{a}{2}\langle 112\rangle$ would dissociate into two perfect $\frac{a}{2}\langle 110\rangle$ dislocations separated by an APB. Each $\frac{a}{2}\langle 110\rangle$ may dissociate into two $\frac{a}{6}\langle 112\rangle$ Shockley partials separated either by a superlattice intrinsic stacking fault (SISF) or a complex stacking fault (CSF). Both faults are intrinsic and have the same stacking sequence: ABCBCABC. In CSF the material has wrong chemistry, similar to an APB, which combined with a broken stacking sequence has higher fault energy than both APB and SISF.

The total Burgers vector $\mathbf{b}$ is determined by three field variables η_1, η_2 and η_3, which define the respective contributions of the principal Burgers vectors $\mathbf{b}_1 = \frac{a}{2}[0\bar{1}1]$, $\mathbf{b}_2 = \frac{a}{2}[10\bar{1}]$ and $\mathbf{b}_3 = \frac{a}{2}[\bar{1}10]$.

$$\mathbf{b} = \eta_1\mathbf{b}_1 + \eta_2\mathbf{b}_2 + \eta_3\mathbf{b}_3 \tag{5}$$

The gamma surface equation can therefore be expressed in terms of the field variables by substituting the following into $\gamma(y,z)$ to give $\gamma(\eta_1,\eta_2,\eta_3)$:

$$y = (-\eta_1 + \eta_3)\sqrt{3}b/2 \tag{6a}$$
$$z = (-\eta_1 + 2\eta_2 - \eta_3)b/2 \tag{6b}$$

Since the system studied is described by non-conserved fields (*i.e.* η is a long range order parameter), its temporal evolution is given by the time-dependent Ginzburg-Landau equation:

$$\frac{\partial\eta(\mathbf{r},t)}{\partial t} = -M\frac{\delta F_{total}}{\delta\eta(\mathbf{r},t)} \tag{7}$$

The relaxation constant M is a mobility term, which for the purpose of this study was selected to be unity. Dislocation mobility in a material is a complex parameter to describe and depends strongly on the conditions and dislocation type. In some cases, dislocations may propagate through a material at the Raleigh velocity [12], in others, slip can occur in a relatively slow viscous manner [13].

Using the model, the evolution of $a\langle 112\rangle$ dislocation ribbons was investigated at different values of applied tensile stress. Pure edge ribbons as well as of those with a 30° screw component were studied. A ribbon was introduced as a pair of identical $\frac{a}{2}\langle 112\rangle$ dislocations. Two precipitate geometries of equivalent

area were considered: a single triangular section through the corner of a cubic precipitate, and a single circular section through a spherical precipitate. The two sections represented the shape of the precipitates in alloys with high and low lattice parameter misfit respectively. However, misfit stresses were not incorporated into the model, as this presents a more difficult problem to solve. The simulations carried out used periodic boundary conditions and a system size of $460 \times 180 \times 32$.

The model assumed elastic homogeneity, whereby both phases had identical elastic constants $c_{11} = 224$, $c_{12} = 148$ and $c_{44} = 125$ GPa obtained for Ni_3Al by Kayser and Stassis [14]. Furthermore the elastic constants were reduced by a factor of 800 to increase the microstructural evolution rate, as dislocations glide faster through a less stiff material. This modification gave tighter cores, especially in in the case of $\frac{a}{2}\langle 110\rangle$ dislocations propagating through the matrix phase. In essence, this created an artificial scaling effect. The simulations were repeated without this reduction modification to verify the results. In both cases, the same overall shear modes were observed and, even though some individual dislocation dissociation differed slightly. For illustration purposes, the former set of the results will be discussed.

3 Results and Discussion

For illustration purposes, the 'Thompson tetrahedron' notation has been used to describe the dislocation configurations observed in the simulations. All simulations were done on the (111) plane, which in this notation system corresponds to the ABC plane. The possible burgers vectors are described as follows:

$$AB = \tfrac{a}{2}[\bar{1}10] \qquad BA = \tfrac{a}{2}[1\bar{1}0]$$
$$AC = \tfrac{a}{2}[01\bar{1}] \qquad CA = \tfrac{a}{2}[0\bar{1}1]$$
$$BC = \tfrac{a}{2}[10\bar{1}] \qquad CB = \tfrac{a}{2}[\bar{1}01]$$
$$A\delta = \tfrac{a}{6}[\bar{1}2\bar{1}] \qquad \delta A = \tfrac{a}{6}[1\bar{2}1]$$
$$B\delta = \tfrac{a}{6}[2\bar{1}\bar{1}] \qquad \delta B = \tfrac{a}{6}[\bar{2}11]$$
$$C\delta = \tfrac{a}{6}[\bar{1}\bar{1}2] \qquad \delta C = \tfrac{a}{6}[11\bar{2}]$$

3.1 Effect of applied stress on γ' cutting mechanism by mixed screw-edge dislocation

Figures 3 and 4 present observations obtained using the model at applied stresses of 750 and 1250 MPa respectively. In both cases, each perfect $3C\delta$ dislocations introduced into the matrix dissociates into one CB and a CA. The first of the two, starts off leading because it experiences a greater resolved stress. As the system evolution progresses significant differences are observed between the two cases. Figure 3 shows γ' precipitate cutting by stacking fault shear. In contrast, Figure 4 shows a transition of cutting mode to shear by APB pairs.

In both figures, three characteristic stages of dislocation configuration evolution are presented. Each stage is illustrated using three separate diagrams, from left to right. First, a false colour map of the crystal free energy derived by the model is shown (left). High and low energies are represented by red and blue ends of the colour spectrum respectively. A schematic of the configuration observed in each energy map is presented (centre) to identify the individual faults and matrix dislocations. Finally, the dislocation core structure profile taken through the longest cross-section of the γ' precipitate is plotted (right). The position of the profile is marked by (red) dotted-dashed line on the schematic of the first stage.

At 0750 MPa deformation of the γ' phase proceeds first by the entry of the leading CB dislocation without dissociation into partials. The APB left in its wake inhibits the cutting through the $L1_2$ ordered phase, Figure 3(a). Subsequently, the first CA and second CB perfect dislocations enter the γ', Figure 3(b). These dissociate *via* the following respective reactions, as dictated by the γ-surface:

$$CA \rightarrow \delta A + \mathbf{SISF} + C\delta \tag{8}$$

$$CB \rightarrow \delta B + \mathbf{CSF} + C\delta \tag{9}$$

The Shockley partials in the first pair above are separated by a SISF and by a CSF in the second. The pairs themselves are, in turn, separated by narrow region of APB. This small separation agrees closely with TEM observations [2] in 2^{nd} generation superalloys. In the case of the model the close separation is explained by the fact that the CB dislocation experiences a greater resolved stress than the CA before it. As a result, it catches up with the dislocation in front of it and closes up the APB within the separation region. The comparatively high fault energy of the APB, also contributes to the speed of its collapse.

The trailing $C\delta$ Shockley partial in Equation (9) leaves behind APB. With three of the $\frac{a}{2}\langle 110\rangle$ dislocations inside the γ' precipitate, there are four high

energy planar faults: three APBs and a CSF. Propagating these acts to retard the overall cutting process. However, the precipitate is not large enough to pin the entire configuration at the given stress. Furthermore, the CSF and APB regions contract in favour of the low energy SISF which expands.

Finally, the last CA dislocation enters the precipitate. Upon entering, its propagation through the γ' phase is rapidly promoted because it reverts the crystal to a perfect state. It does not dissociate into Shockley partials. No dislocation debris is left at the particle-matrix interface.

In the 1250 MPa stress condition, a similar dislocation cutting sequence is observed initially, Figure 4(a). However, interaction between the first CA and second CB dislocations differs signifacantly. When, the faster CB catches up with the CA in the matrix, the two dislocations swap order, Figure 4(b). The trailing dislocation effectively overtakes the leading, due to a higher resolved stress acting on it.

$$CA + CB \rightarrow CB + CA \tag{10}$$

The observed phenomenon could also be interpreted as the swapping of Burgers vectors between the two dislocations. That said, PFM only gives the thermodynamics of the dislocation interactions. The details of the observed process should be verified using mechanical models such as molecular dynamics (MD) and discrete dislocation dynamics (DDD), which are beyond the scope of this work.

This new dislocation order gradually 'unzips' from the matrix phase through the precipitate. In the process, the SISF, CSF and the APB between them are replaced by perfect crystal, Figure 4(c). The ultimate outcome of these dislocation reactions is the transformation of the shearing mode. Now the γ' precipitate is cut by two pairs of identical $\frac{a}{2}\langle 110\rangle$ dislocations separated by a band of perfect crystal. Within each pair the dislocations are separated by an APB, which acts against their mutual repulsion. The original overall Burgers vector of $6C\delta$ is retained. In the γ' the overall dislocation core structure transforms as follows:

$$\begin{aligned} CB + \mathbf{APB} + (\delta A + \mathbf{SISF} + C\delta) + \mathbf{APB} + \\ + (\delta B + \mathbf{CSF} + C\delta) + \mathbf{APB} + CA \rightarrow \\ \rightarrow CB + \mathbf{APB} + CB + \mathbf{PC} + CA + \mathbf{APB} + CA \end{aligned} \tag{11}$$

Figure 6 demonstrates the differences in $6C\delta$ dislocation ribbon configuration during γ' cutting for a range of different stresses. Configurations are imaged at the point where the entire ribbon has entered the precipitate. This corresponds to shorter times as the stress is increased. A transition from stacking fault shear to shear by APB pairs is clearly visible. The SISF area becomes progressively smaller with increasing stress. The transition stress for the trian-

gular precipitate studied must be between 750-1000MPa, which corresponds to the low temperature (≈0-600°C) yield stress of cast single crystal blade superalloys such as CMSX-4, SRR-99, RR-2000 and CMSX-10 [13].

3.2 Effect of orientation on γ' cutting mechanism

To verify that the change in shearing mode occurs due to a difference in resolved shear stress experienced by the dislocations making up the mixed edge-screw $a\langle 112\rangle$ ribbon, a pure edge $a\langle 112\rangle$ with a Burgers vector of $6A\delta$ was studied for comparison over the same range of applied stresses. The dislocations AC and and AB experienced equal resolved shear stresses. The results obtained at 1250MPa are shown in Figure 5.

The first observation difference can be observed immediately (Figure 5(a)), because in pure edge configuration the $3A\delta$ ribbons are stable in the matrix phase when away from precipitates and do not dissociate into $\frac{a}{2}\langle 110\rangle$ dislocations as is observed in Figures 3 and 4. Each $3A\delta$ does, however, dissociate into a $2A\delta$ followed by an $A\delta$. The two partial dislocations are separated by an ISF, which is shown well in Figure 5(a). The $2A\delta$ partial dislocation does not dissociate into a pair of $A\delta$ partials because they would be separated by high energy fault with A/A stacking.

As soon as the leading $3A\delta$ enters the γ' precipitate, it transforms to an AB dislocation, which leaves behind APB and is followed by a δC and $A\delta$ partial dislocations separated by SISF:

$$3A\delta \rightarrow AB + \mathbf{APB} + (\delta C + \mathbf{SISF} + A\delta) \tag{12}$$

The transformation of the $3A\delta$ in the γ' precipitate to effectively an AB dislocation followed by an AC, causes the transformation to occur in the matrix as well. It proceeds in an 'unzipping' manner from the precipitate outwards (Figure 5(a)). As the first $3A\delta$ dislocation cuts through the precipitate phase it leaves behind APB that inhibits its overall propagation. The trailing $A\delta$ partial lags behind causing the low energy SISF to expand in place of the APB.

As the second $3A\delta$ dislocation enters the γ' it also undergoes a transformation to an AB dislocation followed by an AC (Figure 5(b)). However it is the AB dislocation that is dissociated into partials δB and $A\delta$ separated by a very constricted CSF. The AB leaves APB in its wake which is reverted back to perfect crystal by the last AC.

$$3A\delta \rightarrow (\delta B + \mathbf{CSF} + A\delta) + \mathbf{APB} + AC \tag{13}$$

As with the first $3A\delta$, the transformation of the second also unzips through the matrix phase.

For the pure edge ribbon, exactly the same dislocation configuration was observed over the studied range of applied stresses of 500-2000MPa. The AB and AC dislocations formed from the two $3A\delta$ ribbons all experience the same resolved stress and hence propagate at the same rate through the material. Increasing the applied stress only had a constricting effect on the whole configuration, reducing the separation between all of the dislocations.

It can be concluded that dislocation character does play a significant role in the cutting process. A pure edge ribbon, will always cut the γ' precipitates by stacking fault shear. However, in a real turbine blade material, dislocations are loops and their character varies along the perimeter. Shear by APB pairs will become prevalent at higher stresses and greater screw components.

From the gamma surface in Figure 2, one may see the alternative dissociation of the first and second $3A\delta$ dislocations respectively:

$$3A\delta \rightarrow AC + \mathbf{APB} + (\delta B + \mathbf{SISF} + A\delta) \tag{14}$$

$$3A\delta \rightarrow (\delta C + \mathbf{CSF} + A\delta) + \mathbf{APB} + AB \tag{15}$$

This symmetry related configuration is equally valid, and which of the two is chosen should depend on the mis-orientation of the stress relative to the Burger's vector. A slight mis-orientation caused by rounding-off error when defining the system axes favoured in the configuration observed in the phase field simulation.

3.3 Effect of γ' precipitate shape on cutting mechanism

A separate study was carried out to investigate the effect of precipitate shape on the mechanism of dislocation cutting and resistance to shear. A γ' precipitate with a circular cross section and an area equivalent to the triangular sections described in the earlier sections was used. It was subjected to shear by the same pair of mixed edge-screw $3C\delta$ dislocations over a range of applied stresses of 500-2000MPa. The circular precipitate represents the case of low lattice parameter misfit between matrix and precipitate.

The results show a similar transition from stacking fault shear to shear by APB pairs, as with the triangular precipitate section. When some threshold stress, between 750 and 1000MPa, is exceeded, the difference in resolved stress causes the third dislocation to overtake the second. However, this reordering is unable to 'unzip' through the γ' precipitate at 1000MPa and the shearing mode is still stacking fault shear. At 1250MPa there is still no penetration at the widest

section of the precipitate. But when the middle two dislocations reach the far end of the precipitate some penetration occurs, assisted by mutual attraction of dislocations at opposing nodes.

In the case of the triangular precipitate section, transition to APB shear occurs at a lower stress for the inclined RHS rather than the straight LHS. Therefore, it can be seen that the ability of the 'unzipping' process to occur in the precipitate depends on the angle that the reordered dislocations in the matrix make with the precipitate-matrix interface in the direction of travel. The minimum angle depends on the value of the applied stress. At some critical value of the angle, the precipitate geometry makes the change in planar fault configuration energetically favourable, hence allowing 'unzipping'.

3.4 Comparison with experimental observations

Building on the work of Kear *et al.* [15–17], Pollock and Argon [18] and TEM observations, Rae and Reed [2] suggest that primary creep at low temperatures (750-850 °C) and high stresses (≈750 MPa) in CMSX-4 proceeds first by the nucleation of sufficient $\frac{a}{2}\langle 110\rangle$ dislocations. These combine into $a\langle 112\rangle$ dislocation ribbons, *via* reactions like:

$$2 \times [BA + BC] \rightarrow 2 \times 3B\delta \rightarrow 6B\delta \tag{16}$$

This nucleation/incubation phase accounts for the low initial creep rates observed. During cutting of the γ' precipitates, it is hypothesised that the the ribbon dissociates as follows:

$$\begin{aligned} 6B\delta \rightarrow (2B\delta + \mathbf{SISF} + B\delta) + \mathbf{APB} + \\ + (B\delta + \mathbf{SESF} + 2B\delta) \end{aligned} \tag{17}$$

This is an attractive model. It accounts for the low initial creep rate observed under the described stress-temperature conditions. Also, the $a\langle 112\rangle$ ribbons can propagate through the microstructure without leaving dislocation debris. This gives rise to the rapid increase in strain rate observed following incubation. The subsequent hardening of the material at the end of primary creep is explained by simultaneous $\frac{a}{2}\langle 110\rangle$ deformation of the matrix. The matrix dislocations that do not nucleate as ribbons will act as Lomer locks as their population increases.

At stresses below ≈10% of the theoretical yield, the present PFM work sug-

gests the following reaction for a mixed edge-screw dislocation ribbon:

$$\begin{aligned} 2 \times 3B\delta \rightarrow & 2 \times [BC + BA] \rightarrow BC + \mathbf{APB} + \\ & + (\delta A + \mathbf{SISF} + B\delta) + \mathbf{APB} \\ & + (\delta C + \mathbf{CSF} + B\delta) + \mathbf{APB} + BA \end{aligned} \tag{18}$$

As shown in Figure 2, this corresponds to a low stacking fault energy path across the γ-surface for Ni_3Al. High energy maxima are avoided where possible.

The key difference from the Kear model is the absence of the SESF, which has the stacking sequence ABCBABC. The γ-surface used in this work does not account for the possibility of a change in stacking sequence on planes adjacent to the primary slip-plane. Its position is taken on the single layer γ-surface by the highest energy fault labelled A/A'. The stacking sequence is ABCAABC where the two overlapping atoms AA are both aluminium. This is a combination of the most energetically unfavourable stacking with violation of nearest neighbour bonds.

The absence of realistic extrinsic faults is therefore a key limitation of the described phase field model in treating the Primary Creep problem. To model the phenomenon more accurately the crystal free energy must an effective γ-surface that does allow for such defects.

Future and ongoing studies aim to incorporate the work of Voskoboinikov and Rae [19]. It has shown that extrinsic faults in Ni_3Al have three forms. The SESF is equivalent to two overlapping SISFs (*i.e.* SISF/SISF), however CSF/SISF and CSF/CSF are also possible. The latter has the highest fault energy. It is impossible to obtain the SESF by pure shear, this only gives CSF/CSF, which has not been observed experimentally. However some form of atomic shuffle is needed to produce the lower energy SESF. In the work of Unocic *et al.* [20], a possible mechanism of unzipping through vacancy migration is proposed. Alternatives to this could be other diffusional processes or thermally activated shear.

At stresses of above ≈10% of the theoretical yield, cutting of the γ' precipitates occurs by APB pairs instead of a mixed screw-edge $a\langle 112 \rangle$ super-dislocation:

$$\begin{aligned} 2 \times 3B\delta \rightarrow & 2 \times [BC + BA] \rightarrow BC + \mathbf{APB} + BC + \\ & + \mathbf{PC} + BA + \mathbf{APB} + BA \end{aligned} \tag{19}$$

Thus the case in Equation (18) reproduces partially mechanisms observed in primary creep specimens of superalloys at elevated temperatures and sub-yield applied stresses. According to Décamps *et al.* [21], a large numbers of SISFs are observed in tensile creep specimens at intermediate temperatures.

There are no SESFs, which are geometrically favourable in compression. In comparison, Equation (19) reproduces dislocation configurations observed in these materials after tensile tests at room temperature . Although the model lacks the necessary physics to reproduce extrinsic faults, the overall findings are consistent with the hypotheses and findings of Kear *et al.*

It is also worth noting that the model predicts the existence of tight $\frac{a}{2}\langle 112\rangle$ dislocations in the matrix phase, which can be are observed in TEM. In Figure 1 these can be seen as thin bands where the ribbon extends through the γ phase between precipitates.

4 Conclusion

The $a\langle 112\rangle$ ribbon cutting mechanism for primary creep of single crystal nickel superalloys suggested by Kear has been evaluated using Phase Field Microelasticity. The findings can be summarised as follows:

(1) The γ' shearing mode has been found to exhibit a strong stress dependence. A transition from stacking fault shear to cutting by APB pairs is observed for mixed screw-edge dislocation ribbons at approximately 10% of the theoretical yield. This is achieved by reordering of dislocations, which allows those with greatest resolved stress to "overtake" and lead.
(2) The γ' shearing mode exhibits an orientation dependence. A pure edge $a\langle 112\rangle$ ribbon normal to the applied stress always displays the same dissociation sequence regardless of the stress.
(3) The angle between the dislocation line and the matrix-precipitate interface determines whether 'unzipping' can occur to change the shearing mode at a given stress.
(4) The inability to model extrinsic faults limits the possible fault configurations and is a significant limitation. The described model is only able to model intrinsic faults, and the material is unable to attain the lowest possible energy fault configuration seen in TEM. However, it does reproduce the case of tension creep at intermediate temperatures as well as room temperature tensile deformation.

PFM with γ-surface based $F_{crystal}$ is a promising tool for studying in-plane dislocation interactions governing the strength of both precipitation and order hardened alloys.

5 Acknowledgements

VV would like to thank YW for funding his stay at OSU in summer 2006. VV also extends his gratitude to all members of CAMM under of Dr H. Fraser as well as Dr N. Zhou for significant assistance with equipment and theoretical background. Funding from EPSRC and MOD under grants EP/D04619X/1, EP/C536312/1 and GR/T26344/01 is acknowledged.

References

[1] R. C. Reed, N. Matan, D. C. Cox, M. A. Rist, C. M. F. Rae, Acta Mater. 47 (1999) 3367–3381.

[2] C. M. F. Rae, R. C. Reed, Acta Mater, 55 (2006) 1067–1081.

[3] Y. U. Wang, Y. M. Jin, A. M. Cuitino, A. G. Khachaturyan, Acta Mater. 49 (2001) 1847–1857.

[4] C. Shen, Y. U. Wang, Acta Mater. 52 (2004) 683–691.

[5] A. G. Khachaturyan, Theory of structural transformations in solids, Dover Publications Inc., 1983.

[6] J. D. Eshelby, Proc. R. Soc. A 241 (1957) 376–396.

[7] G. Schoeck, S. Kohlhammer, M. Fahnle, Phil. Mag. L. 79 (1999) 849–857.

[8] G. Schoeck, Private communication.

[9] P. Veyssiére, J. Doin, P. Beuchamp, Phil. Mag. A 51 (1985) 469–483.

[10] M. J. Mills, Private communication.

[11] J. Li, Private communication.

[12] J. Hirth, J. Lothe, Theory of Dislocations, John Wiley & Sons, 1982.

[13] R. Reed (Ed.), The Superalloys, Fundamentals and Applications, Cambridge University Press, 2006.

[14] F. X. Kayser, C. Stassis, Phys. Stat. Sol. A 64 (1981) 335–342.

[15] B. H. Kear, A. F. Giamei, G. R. Leverant, J. M. Oblak, Scripta Met. 3 (1969) 123–130.

[16] B. H. Kear, A. F. Giamei, G. R. Leverant, J. M. Oblak, Scripta Met. 3 (1969) 455–460.

[17] B. H. Kear, J. M. Oblak, A. F. Giamei, Met. Trans. 1 (1970) 2477–2486.

[18] T. M. Pollock, A. S. Argon, Acta metall. mater. 40 (1992) 1–30.

[19] R. E. Voskoboinikov, C. M. F. Rae, IOP Conf. Ser. : Mat. Sci. & Eng.Preprint submitted.

[20] R. R. Unocic, L. Kovarik, C. Shen, P. M. Sarosi, Y. Wang, J. Li, S. Gosh, M. J. Mills, in: "Superalloys" Proceedings, 2008, pp. 377–385.

[21] B. Décamps, A. J. Morton, M. Condat, Phil. Mag. A 64 (1990) 641–668.

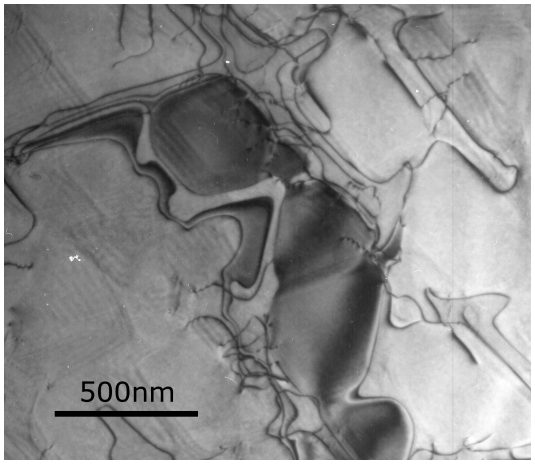

Fig. 1. TEM micrograph showing a {111} section through TMS-82+ superalloy deformed in tension to 1.4% strain at 750°C and 750MPa. Evidence of primary creep is visible: γ channels are populated with $\frac{a}{2}\langle 110\rangle$ dislocations, an $a\langle 112\rangle$ ribbon has nucleated in the matrix and sheared several γ' precipitates leaving intrinsic and extrinsic faults.

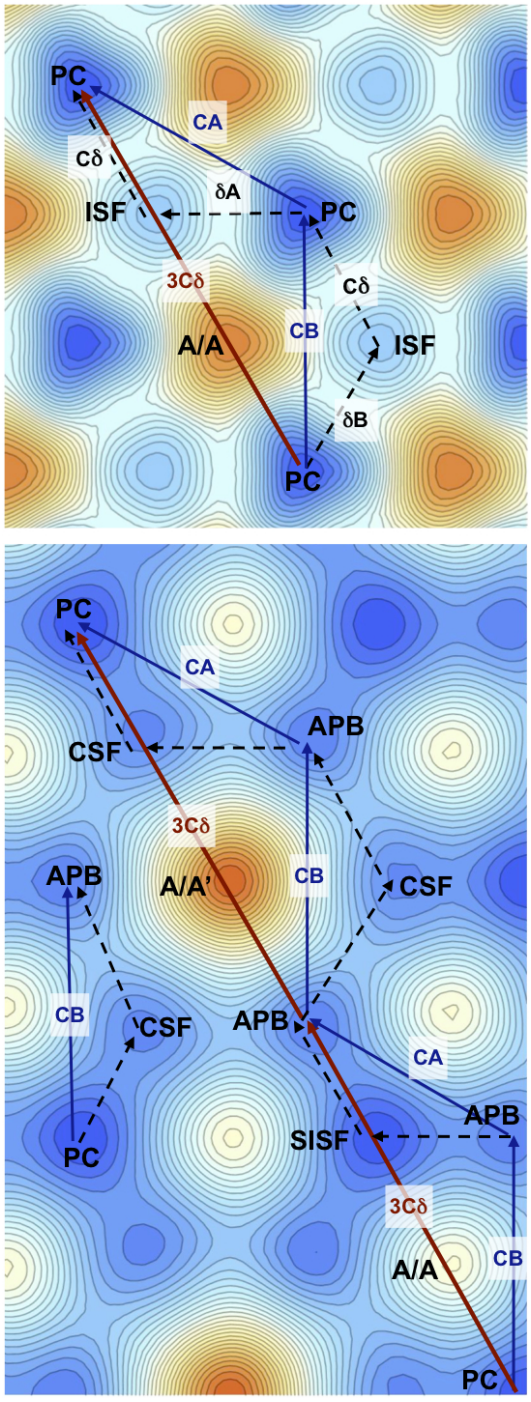

Fig. 2. γ-surfaces for pure Ni (top) and Ni_3Al (bottom).

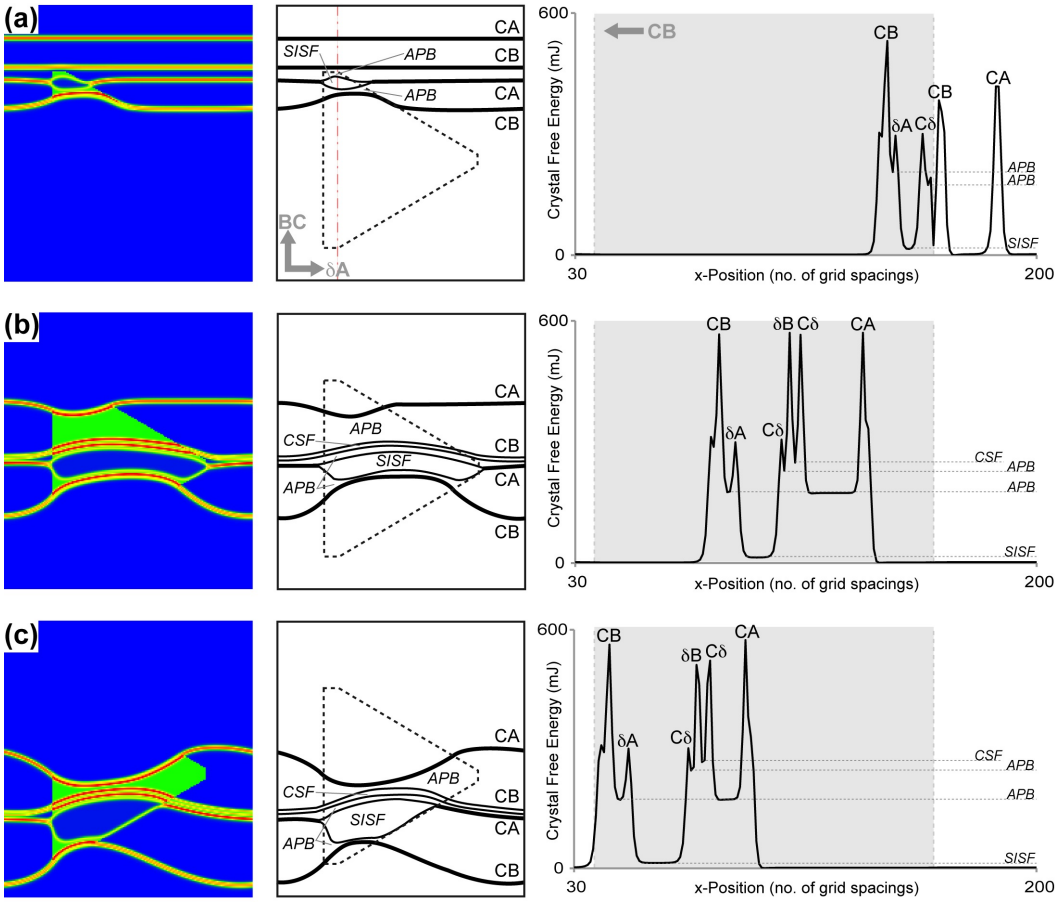

Fig. 3. Analysis of results for 750MPa applied stress showing γ' shearing with stacking faults. Evolution stages at t =520, 1840 and 2680 are shown, with Δt=0.1.

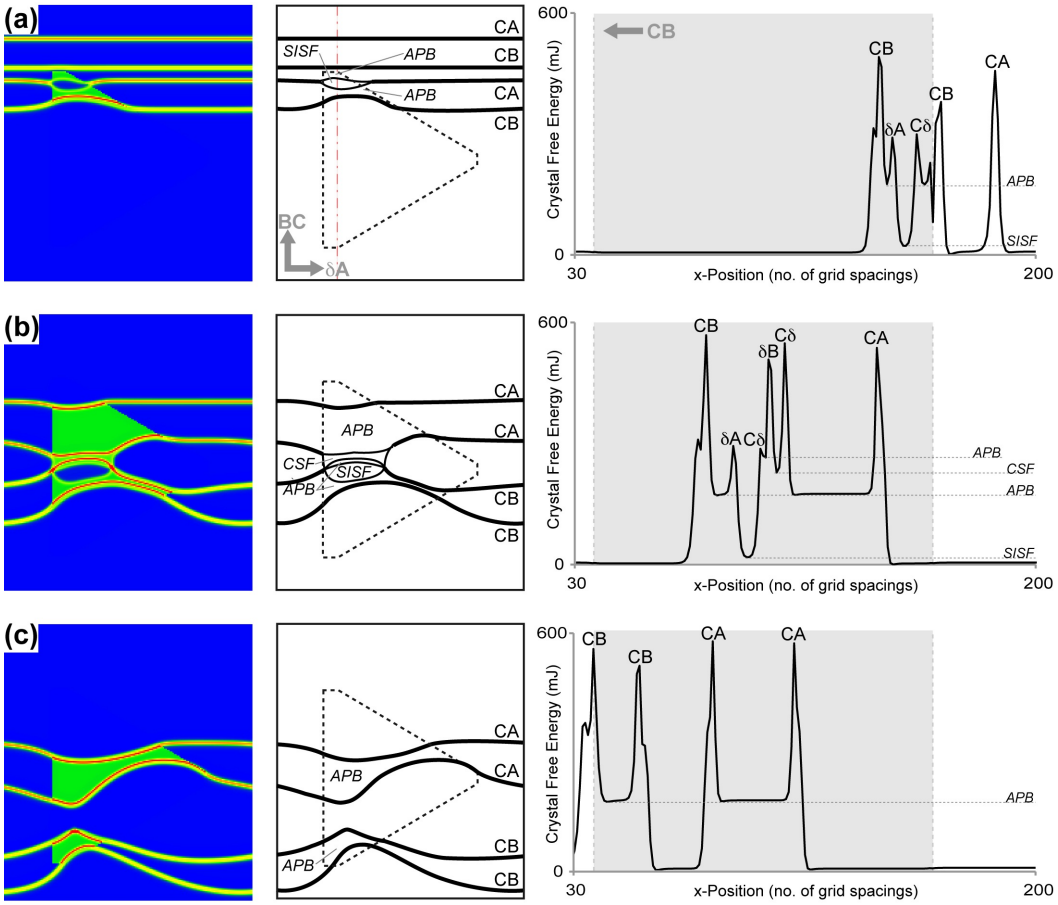

Fig. 4. Analysis of results for 1250MPa applied stress. A transition from stacking fault shear to shear by APB pairs occurs. Evolution stages at t =320, 1080 and 1520 are shown, with Δt=0.1.

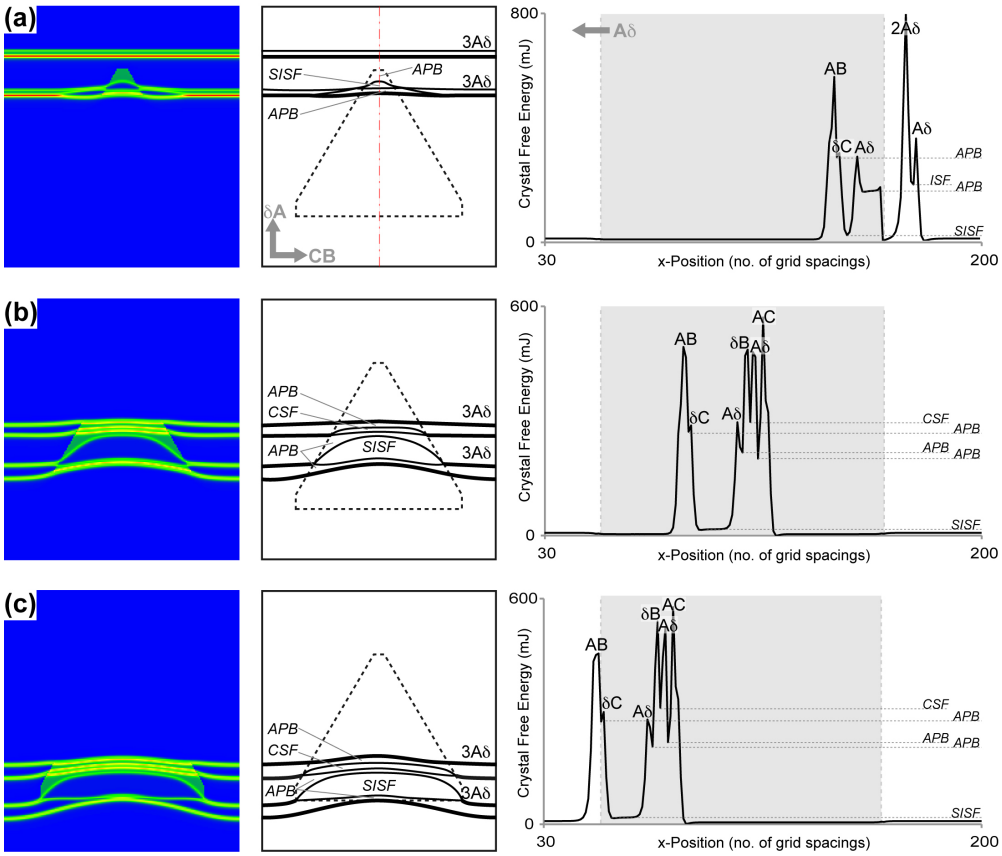

Fig. 5. Analysis of results for 1250MPa applied stress. A transition from stacking fault shear to shear by APB pairs occurs. Evolution stages at t =320, 1080 and 1520 are shown, with Δt=0.1.

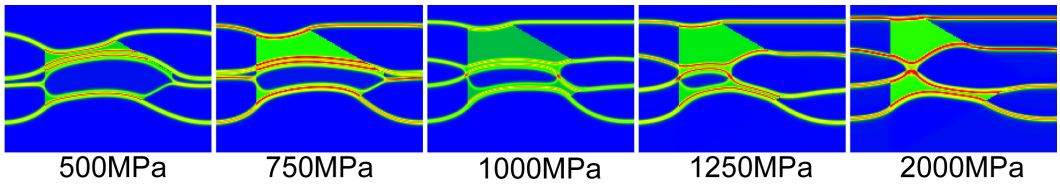

Fig. 6. Comparison of dislocation and fault configurations showing a transition between mechanism with increasing stress.

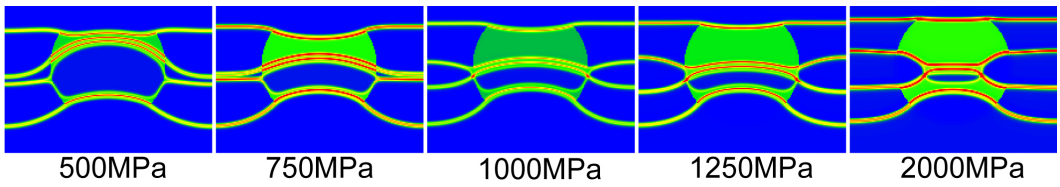

Fig. 7. Comparison of dislocation and fault configurations showing a transition between mechanism with increasing stress.